Materials Physics and Mechanics. 2023;51(1): 42-60
Research article
http://dx.doi.org/10.18149/MPM.5112023_5

Submitted: February 3, 2022
Approved: November 9, 2022
Accepted: January 13, 2023

Wave propagation in a nonlocal rotating micropolar piezoelectric solid

Baljeet Singh [1] ✉, Asha Sangwan [2], Jagdish Singh [3]

[1]Department of Mathematics, Post Graduate Government College, Sector-11, Chandigarh-160011, India

[2]Department of Mathematics, Government College, Sampla, Rohtak-124001, Haryana, India

[3]Department of Mathematics, Maharshi Dayanand University, Rohtak,-124001, Haryana, India

✉ bsinghgc11@gmail.com

Abstract. The nonlocal theory of elasticity is applied to formulate the governing equations of nonlocal micropolar piezoelectric material in a rotating frame. The governing equations are specialized for a plane and solved to show the existence of three coupled plane waves. Reflection of a coupled longitudinal displacement wave is considered at a stress-free surface of half-space containing the micropolar piezoelectric material. For the incidence of coupled longitudinal displacement waves, the expressions of reflection coefficients and energy ratios for reflected waves are derived. A quantitative example is set up to illustrate the effects of rotation and nonlocal parameters on the reflection coefficients and energy ratios in a given range of the angle of incidence.

Keywords: plane waves, nonlocality, rotation, reflection coefficients, energy ratios

Citation: Singh Baljeet, Sangwan Asha, Singh Jagdish. Wave propagation in a nonlocal rotating micropolar piezoelectric solid. *Materials Physics and Mechanics*. 2023;51(1): 42-60. DOI: 10.18149/MPM.5112023_5.

Introduction

Plane wave reflection and refraction phenomenon are extensively used to conduct non-destructive testing or non-destructive evaluation of composites for characterizing/mapping subsurface defects and assessing the in-situ condition of structural components without reforming the original features of the composites in a non-tarnish way. Elastic wave propagation problems in layered media have been discussed by several authors. Prominent among them are Knott [1], Jeffreys [2], Gutenberg [3], Ergin [4], Ewing et al. [5], and Achenbach [6].

Piezoelectric materials find their utility as sensors and actuators in many applications involving signal transmission. Various analytical studies on wave characteristics in piezoelectric materials were investigated (Kyame [7], Pailloux [8], Cheng and Sun [9], Auld [10], Alshits et al. [11], Parton and Kudryavtsev [12], Every and Neiman [13], Alshits and Shuvalov [14], Wang [15], Yang [16], Pang et al. [17], Darinskii et al. [18], Burkov et al. [19], Abd-alla and Al-sheikh [20], Singh [21], Kuang and Yuan [22], Yuan and Zhu [23], Guo and Wei [24], Guo et al. [25], Othman et al. [26], Singh and Singh [27], Jiao et al. [28], Sahu et al. [29], Singh et al. [30], Liu et al. [31].

The translation and rotation of a moving object can be sensed by accelerometers and gyroscopes, respectively. These motion sensors are used as an important tool in smart weapon systems, video cameras, automobiles, robotics, navigation, and machine control. Recently, vibratory gyroscopes made up of piezoelectric materials have been a centre of research. The governing equations with Centrifugal and Coriolis accelerations for a rotating piezoelectric body are responsible for observing the fundamental nature of the piezoelectric gyroscope. The

rotational effects on plane waves in an isotropic medium were observed by Schoenberg and Censor [32]. According to White [33], the rotational effect on frequency or wave speed provides valuable inputs for acoustic sensors design. In particular, the rotation-induced frequency shifts have been applied to manufacture the gyroscopes (Tiersten et al. [34], Tiersten et al. [35], Wren and Burdess [36]).

In recent years, the materials and structures have been considered on a nano-scale to meet the requirement of various acoustic devices to have greater sensitivity and storage within the smaller structure. The applications of nonlocal theory help to explain and predict physical phenomena at small length scales. Edelen et al. [37], Eringen and Edelen [38], and Eringen [39] developed the nonlocal elasticity theory characterized by the presence of nonlocality residuals fields like body force, mass, entropy, and internal energy. Eringen [40,41] applied the nonlocal elasticity theory to investigate plane waves in elastic media. Thereafter, various researchers investigated wave propagation problems by using nonlocal elasticity theories. More recent works are cited as Roy et al. [42], Khurana and Tomar [43,44], Singh [45,46], Kaur and Singh [47], Liu et al.[31] and Tung [48].

The micropolar elasticity extends classical elasticity with extra independent degrees of freedom for local rotation. Eringen [49-51] introduced linear micropolar elasticity, where the motions of the particles are represented by the displacement and micro-rotation vectors. The theory of micropolar elasticity was further applied by various researchers in piezoelectric materials. For example, the works of Cracium [52], Ciumasu and Vieru [53], Vieru and Ciumasu [54], Zhilin and Kolpakov [55], Aouadi [56], and Gales [57] are cited for reference. Recently, the piezoelectricity of micropolar materials was used to explore the plane and surface wave characteristics by Singh and Sindhu [58,59], Sangwan et al. [60], Singh et al. [61] and Bijarnia et al. [62]. The main motivation of this paper is to apply the nonlocal elasticity theory for the investigation of rotational effects on plane waves in the micropolar piezoelectric medium.

In section 2, the governing equations of a transversely isotropic, rotating, nonlocal micropolar piezoelectric medium are specialized for a plane. In section 3, the existence of three coupled plane waves is discussed. In section 4, a reflection phenomenon of coupled longitudinal displacement wave from a traction-free boundary of a semi-infinite space is considered. The expressions for reflection coefficients and energy ratios are derived. In section 5, some special cases are discussed. In section 6, a quantitative example of the model is set up to graphically illustrate the effects of rotation and nonlocality on the speeds, amplitude ratios, and energy ratios in a given range of propagation angles.

Governing equations

We consider a nonlocal rotating micropolar piezoelectric solid material with constant angular velocity $\vec{\Omega} = \Omega \hat{n}$, where $\hat{n}$ is a unit vector along the axis of rotation. The fixed coordinate system in the rotating solid introduces Centripetal acceleration $\vec{\Omega}\times\left(\vec{\Omega}\times\vec{u}\right)$ by virtue of time-changing motion only and Coriolis acceleration $\left(2\vec{\Omega}\times\dot{\vec{u}}\right)$. According to Schoenberg and Censor [32], Eringen and Edelen [38], Eringen [39], and Aouadi [56], the fundamental system of field equations without body forces and body couples for the linear theory of rotating nonlocal micropolar piezoelectric solids are formulated as

(a) The equations of the motion

$$\sigma_{ji,j} = \rho\left[\ddot{u}_i + \left\{\vec{\Omega}\times\left(\vec{\Omega}\times\vec{u}\right)\right\}_i + \left(2\vec{\Omega}\times\dot{\vec{u}}\right)_i\right], \tag{1}$$

$$m_{ik,i} + \varepsilon_{ijk}\sigma_{ij} = \rho j\ddot{\phi}_k, \tag{2}$$

(b) The equations of the electric fields

$$D_{j,j} = q_e,\ E_k = -\psi_{,k}, \tag{3}$$

(c) The constitutive equations

$$\left(1-\varepsilon^2\nabla^2\right)\sigma_{ij} = c_{ijkl}e_{kl} + b_{ijkl}\kappa_{kl} + \lambda_{ijk}E_k, \tag{4}$$

$$\left(1-\varepsilon^2\nabla^2\right)m_{ij} = b_{klij}e_{kl} + a_{ijkl}\kappa_{kl} + \beta_{ijk}E_k, \tag{5}$$

$$D_k = -\lambda_{ijk}e_{ij} - \beta_{ijk}\kappa_{ij} + \gamma_{kj}E_j, \tag{6}$$

(d) The geometrical equations

$$e_{ij} = u_{j,i} + \varepsilon_{ijk}\phi_k,\ \kappa_{ij} = \phi_{j,i}, \tag{7}$$

where ρ is the mass density, ε is the nonlocal parameter, $\vec{u}$ is the displacement vector, $\vec{\phi}$ is the microrotation vector, σ_{ij} is the stress tensor, m_{ij} is the couple stress tensor, j is the micro-inertia, ε_{ijk} is the alternating symbol, D_k is the dielectric displacement vector, q_e is the volume charge density, E_j is the electric field vector, ψ is the electrostatic potential, e_{ij} and κ_{ij} are kinematic strain measures and $a_{ijkl}, b_{ijkl}, c_{ijkl}, \lambda_{ijk}, \beta_{ijk}$ and γ_{jk} are constitutive coefficients. The symbol ∇^2 is the Laplace operator. Subscripts preceded by a comma denote space partial derivatives. The superposed dot denotes time partial derivatives. The constitutive coefficients satisfy the following symmetry relations

$$c_{ijkl} = c_{klij},\ a_{ijkl} = a_{klij},\ \gamma_{ij} = \gamma_{ji}. \tag{8}$$

Now, we consider an infinite linear, homogeneous, and transversely isotropic nonlocal rotating micropolar piezoelectric solid half-space. We take the origin of the rectangular Cartesian coordinate system (x_1, x_2, x_3) on the free surface $x_3 = 0$ and x_3-axis is taken normal to the half-space. The plane of isotropy is taken perpendicular to x_3-axis and the rotation is assumed with constant angular velocity $\vec{\Omega}$ about x_2-axis. For a two-dimensional problem, we consider the following components of displacement vector $\vec{u}$, microrotation vector $\vec{\phi}$, and angular velocity $\vec{\Omega}$

$$\vec{u} = (u_1, 0, u_3),\ \vec{\phi} = (0, \phi_2, 0),\ \vec{\Omega} = (0, \Omega, 0). \tag{9}$$

Using Equation (9) in Equations (1-8), the governing equations for transversely isotropic rotating nonlocal micropolar piezoelectric medium in $x_1 - x_3$ plane reduce to the following system of four partial differentials equations in u_1, u_3, ϕ_2 and ψ

$$A_{11}\frac{\partial^2 u_1}{\partial x_1^2} + (A_{13}+A_{56})\frac{\partial^2 u_3}{\partial x_1 \partial x_3} + A_{55}\frac{\partial^2 u_1}{\partial x_3^2} + K_1\frac{\partial \phi_2}{\partial x_3} - (\lambda_{15}+\lambda_{31})\frac{\partial^2 \psi}{\partial x_1 \partial x_3} = \rho\left(1-\varepsilon^2\nabla^2\right)\left[\frac{\partial^2 u_1}{\partial t^2} - \Omega^2 u_1 + 2\Omega\frac{\partial u_3}{\partial t}\right] \tag{10}$$

$$A_{66}\frac{\partial^2 u_3}{\partial x_1^2} + (A_{13}+A_{56})\frac{\partial^2 u_1}{\partial x_1 \partial x_3} + A_{33}\frac{\partial^2 u_3}{\partial x_3^2} + K_2\frac{\partial \phi_2}{\partial x_1} - \lambda_{15}\frac{\partial^2 \psi}{\partial x_1^2} - \lambda_{33}\frac{\partial^2 \psi}{\partial x_3^2} = \rho\left(1-\varepsilon^2\nabla^2\right)\left[\frac{\partial^2 u_3}{\partial t^2} - \Omega^2 u_3 - 2\Omega\frac{\partial u_1}{\partial t}\right] \tag{11}$$

$$B_{77}\frac{\partial^2 \phi_2}{\partial x_1^2} + B_{66}\frac{\partial^2 \phi_2}{\partial x_3^2} - \chi\phi_2 - K_1\frac{\partial u_1}{\partial x_3} - K_2\frac{\partial u_3}{\partial x_1} = \rho j\left(1-\varepsilon^2\nabla^2\right)\frac{\partial^2 \phi_2}{\partial t^2} \tag{12}$$

$$\lambda_{15}\frac{\partial^2 u_3}{\partial x_1^2} + \lambda_{33}\frac{\partial^2 u_3}{\partial x_3^2} + (\lambda_{15}+\lambda_{31})\frac{\partial^2 u_1}{\partial x_1 \partial x_3} + \gamma_{11}\frac{\partial^2 \psi}{\partial x_1^2} + \gamma_{33}\frac{\partial^2 \psi}{\partial x_3^2} = 0 \tag{13}$$

where

$$\nabla^2 = \frac{\partial^2}{\partial x_1^2} + \frac{\partial^2}{\partial x_3^2},$$

$$A_{11} = C_{1111}, A_{55} = C_{3131},\ A_{13} = C_{1133} = C_{3311},\ A_{56} = C_{3113} = C_{1331}, A_{66} = C_{1313},\ A_{33} = C_{3333},$$

$$K_1 = A_{56} - A_{55} = C_{3113} - C_{3131}, K_2 = A_{66} - A_{56} = C_{1313} - C_{1331}, \chi = K_2 - \mathrm{K}_1, B_{77} = a_{1212},$$

$$B_{66} = a_{3232}, \lambda_{31} = \lambda_{311}, \lambda_{33} = \lambda_{333},\ \lambda_{15} = \lambda_{131} = \lambda_{113},\ \lambda_{35} = \lambda_{313} = \lambda_{331}.$$

Plane waves

The plane harmonic solutions of Equations (10-13) are considered as

$$\{u_1, u_3, \phi_2, \psi\} = \{u_1^*, u_3^*, \phi_2^*, \psi^*\} \exp\{ik(x_1 \sin\theta + x_3 \cos\theta) - i\omega t\}, \tag{14}$$

where $\mathrm{i} = \sqrt{-1}$, k is the wave number, ω is the circular frequency, θ is propagation angle, and v is the propagation speed.

Using Equation (14) in Equations (10-13), we obtain a homogenous system of four equations in u_1^*, u_3^*, ϕ_2^* and ψ^* the non-zero solutions of which require the following condition

$$D_0 \Lambda^3 - D_1 \Lambda^2 + D_2 \Lambda - D_3 = 0, \tag{15}$$

where $\Lambda = \rho\left(\frac{v}{\omega}\right)^2$ and the expressions for $D_j\ (j = 0,1,2,3)$ are given as

$$D_0 = \alpha_5 M_3 \left(M_1^2 + M_2^2\right),$$

$$D_1 = \alpha_5 M_1 M_3 (\alpha_1 + \alpha_2) + \alpha_5 M_1 \left[\left(K_1^*\right)^2 + \left(K_2^*\right)^2\right] + M_1 M_3 \left(\alpha_3^2 + B_3^2\right)$$

$$- \alpha_5 M_2 M_3 (B_2 - B_1) - \alpha_4 \alpha_5 \left(M_1^2 + M_2^2\right),$$

$$D_2 = \left(\alpha_2 \alpha_5 + \alpha_3^2\right)\left(K_1^*\right)^2 + \left(\alpha_1 \alpha_5 + B_3^2\right)\left(K_2^*\right)^2 - \left(2\alpha_3 B_3 + \alpha_5 B_1 + \alpha_5 B_2\right) K_1^* K_2^*$$

$$- \alpha_4 M_1 \left(\alpha_3^2 + B_3^2\right) - \alpha_4 \alpha_5 M_1 (\alpha_1 + \alpha_2) - (B_1 + B_2) \alpha_3 B_3 M_3$$

$$+ \left(\alpha_1 \alpha_3^2 + \alpha_2 B_3^2\right) M_3 + \left(\alpha_1 \alpha_2 - B_1 B_2\right) \alpha_5 M_3 + \alpha_4 \alpha_5 M_2 (B_2 - B_1),$$

$$\mathrm{D}_3 = \alpha_4 \alpha_5 \mathrm{B}_1 \mathrm{B}_2 + (\mathrm{B}_1 + \mathrm{B}_2) \alpha_3 \alpha_4 \mathrm{B}_3 - \alpha_1 \alpha_4 \alpha_3^2 - \alpha_2 \alpha_4 \mathrm{B}_3^2 - \alpha_1 \alpha_2 \alpha_4 \alpha_5,$$

where

$$\alpha_1 = A_{11} \sin^2\theta + A_{55} \cos^2\theta - \left[1 + \left(\Omega^*\right)^2\right] \rho \varepsilon^2 \omega^2,$$

$$\alpha_2 = A_{66} \sin^2\theta + A_{33} \cos^2\theta - \left[1 + \left(\Omega^*\right)^2\right] \rho \varepsilon^2 \omega^2,\quad \alpha_3 = \lambda_{15} \sin^2\theta + \lambda_{33} \cos^2\theta,$$

$$\alpha_4 = B_{77} \sin^2\theta + B_{66} \cos^2\theta - \rho j \varepsilon^2 \omega^2,\quad \alpha_5 = \gamma_{11} \sin^2\theta + \gamma_{33} \cos^2\theta,$$

$$B_1 = \left(A_{13} + A_{56}\right) \sin\theta \cos\theta - 2i\Omega^* \rho \varepsilon^2 \omega^2,\quad B_2 = \left(A_{13} + A_{56}\right) \sin\theta \cos\theta + 2i\Omega^* \rho \varepsilon^2 \omega^2,$$

$$B_3 = \left(\lambda_{15} + \lambda_{31}\right) \sin\theta \cos\theta,\quad K_1^* = iK_1 \cos\theta,\ K_2^* = iK_2 \sin\theta,$$

$$\Omega^* = \frac{\Omega}{\omega},\ M_1 = \left[1 + \left(\Omega^*\right)^2\right] \rho \omega^2,\quad M_2 = 2i\Omega^* \rho \omega^2,\ M_3 = \chi - \rho j \omega^2.$$

The dispersion Equation (15) is a cubic equation in v^2. Three roots v_1, v_2 and v_3 of Equation (15) are found to be real and positive with inequality $v_1 > v_2 > v_3$. These three roots suggest the existence of three plane waves, namely, Coupled Longitudinal Displacement

(CLD), Coupled Transverse Displacement (CTD), and Coupled Transverse Microrotational (CTM) waves with distinct speeds v_1, v_2 and v_3, respectively.

Reflection of Coupled Longitudinal Displacement (CLD) wave

An incident CLD wave propagating with velocity v_1 through the transversely isotropic rotating nonlocal micropolar piezoelectric solid half-space (M) strikes the free surface $x_3 = 0$ making an angle θ_o with negative x_3-axis. The incident CLD wave will generate three reflected waves as CLD, CTD, and CTM waves in medium M. The geometry showing the directions of striking waves and reflected waves is illustrated in Fig. 1.

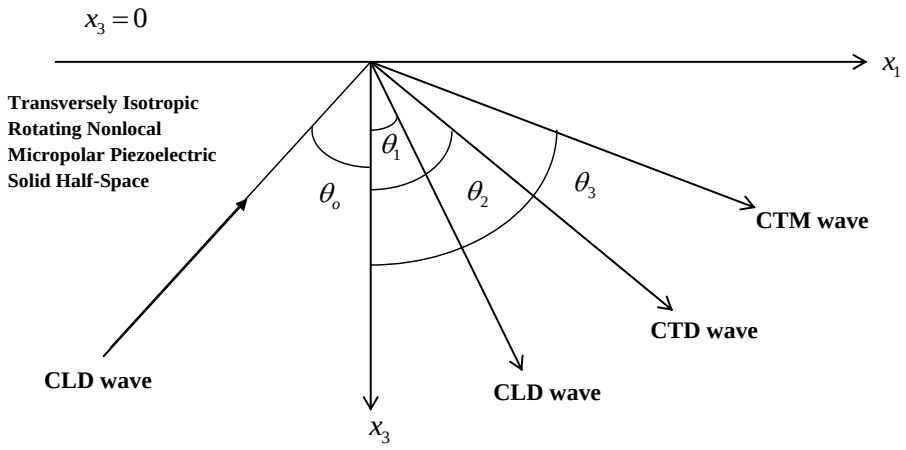

Fig. 1. Geometry of the problem illustrating the striking and reflected waves

The appropriate displacement components u_1, u_3, microrotation component ϕ_2, and electric potential ψ for the incident and reflected waves in medium M are

$$u_1 = A_o \exp\left\{ik_1\left(x_1 \sin\theta_o + x_3 \cos\theta_o\right) - i\omega t\right\} + \sum_{j=1}^{3} A_j \exp\left\{ik_j\left(x_1 \sin\theta_j - x_3 \cos\theta_j\right) - i\omega t\right\}, \tag{16}$$

$$u_3 = \xi_1^* A_o \exp\left\{ik_1\left(x_1 \sin\theta_o + x_3 \cos\theta_o\right) - i\omega t\right\} + \sum_{j=1}^{3} \xi_j A_j \exp\left\{ik_j\left(x_1 \sin\theta_j - x_3 \cos\theta_j\right) - i\omega t\right\}, \tag{17}$$

$$\phi_2 = \eta_1^* A_o \exp\left\{ik_1\left(x_1 \sin\theta_o + x_3 \cos\theta_o\right) - i\omega t\right\} + \sum_{j=1}^{3} \eta_j A_j \exp\left\{ik_j\left(x_1 \sin\theta_j - x_3 \cos\theta_j\right) - i\omega t\right\}, \tag{18}$$

$$\psi = \zeta_1^* A_o \exp\left\{ik_1\left(x_1 \sin\theta_o + x_3 \cos\theta_o\right) - i\omega t\right\} + \sum_{j=1}^{3} \zeta_j A_j \exp\left\{ik_j\left(x_1 \sin\theta_j - x_3 \cos\theta_j\right) - i\omega t\right\}, \tag{19}$$

where the explicit expressions for coupling coefficients $\xi_1^*, \eta_1^*, \zeta_1^*, \xi_j, \eta_j$ and $\zeta_j \left(j = 1,2,3\right)$ are provided in Appendix.

The mechanical boundary conditions applied at $x_3 = 0$ are vanishing of the normal force stress component, tangential force stress component, and tangential couple stress component i.e.,

$$\sigma_{33}=0,\ \sigma_{31}=0,\ \ m_{32}=0, \tag{20}$$

where

$$\left(1-\varepsilon^2\nabla^2\right)\sigma_{33}=A_{13}\frac{\partial u_1}{\partial x_1}+A_{33}\frac{\partial u_3}{\partial x_3}-\lambda_{35}\frac{\partial \psi}{\partial x_1}-\lambda_{33}\frac{\partial \psi}{\partial x_3},$$

$$\left(1-\varepsilon^2\nabla^2\right)\sigma_{31}=A_{56}\frac{\partial u_3}{\partial x_1}+A_{55}\frac{\partial u_1}{\partial x_3}+\left(A_{56}-A_{55}\right)\phi_2-\lambda_{31}\frac{\partial \psi}{\partial x_1}-\lambda_{35}\frac{\partial \psi}{\partial x_3},$$

$$\left(1-\varepsilon^2\nabla^2\right)m_{32}=B_{66}\frac{\partial \phi_2}{\partial x_3}.$$

The displacement components, microrotation component, and electric potential functions given by Equations (16) to (19) satisfy the boundary conditions (20) with the following relations (analogous to Snell's law)

$$k_1\sin\theta_o=k_1\sin\theta_1=k_2\sin\theta_2=k_3\sin\theta_3,\ \ k_1v_1=k_2v_2=k_3v_3 \tag{21}$$

and the following three relations in amplitude ratios of reflected waves are derived as

$$\sum_{j=1}^{3}a_{ij}Z_j=h_i,\quad (i=1,2,3), \tag{22}$$

where $Z_j=\dfrac{A_j}{A_o}$, $(j=1,2,3)$ are amplitude ratios of reflected CLD wave, reflected CTD wave, and reflected CTM wave, respectively and

$$a_{1j}=\frac{\left(A_{13}-\lambda_{35}\zeta_j\right)\sin\theta_o-\left(A_{33}\xi_j-\lambda_{33}\zeta_j\right)f_j^*}{\left(A_{13}-\lambda_{35}\zeta_1^*\right)\sin\theta_o+\left(A_{33}\xi_1^*-\lambda_{33}\zeta_1^*\right)\cos\theta_o},\quad (j=1,2,3)$$

$$a_{2j}=\frac{\left(A_{56}\xi_j-\lambda_{31}\zeta_j\right)\sin\theta_o-\left(A_{55}-\lambda_{35}\zeta_j\right)f_j^*-i\left(A_{56}-A_{55}\right)\left(\dfrac{v_1}{v_j}\right)\left(\dfrac{\eta_j}{k_j}\right)}{\left(A_{56}\xi_1^*-\lambda_{31}\zeta_1^*\right)\sin\theta_o+\left(A_{55}-\lambda_{35}\zeta_1^*\right)\cos\theta_o-i\left(A_{56}-A_{55}\right)\left(\dfrac{\eta_1^*}{k_1}\right)},\quad (j=1,2,3)$$

$$a_{3j}=\frac{\left(\dfrac{\eta_j}{k_j}\right)\left(\dfrac{v_1}{v_j}\right)f_j^*}{\left(\dfrac{\eta_1^*}{k_1}\right)\cos\theta_o},\qquad (j=1,2,3)$$

$$h_1=-1,\ h_2=-1,\ h_3=1,$$

where

$$f_j^*=\sqrt{\left(\frac{v_1}{v_j}\right)^2-\sin^2\theta_o},\qquad (j=1,2,3).$$

Following Achenbach [6], the rate of energy transmission at the interface $x_3=0$ is

$$P^*=\left(1-\varepsilon^2\nabla^2\right)\sigma_{33}\frac{\partial u_3}{\partial t}+\left(1-\varepsilon^2\nabla^2\right)\sigma_{31}\frac{\partial u_1}{\partial t}+\left(1-\varepsilon^2\nabla^2\right)m_{32}\frac{\partial \phi_2}{\partial t}. \tag{23}$$

The time rate of average energy transmission for the respective wave to that of the incident wave, denoted by $E_j\ (j=1,2,3)$ for reflected CLD, reflected CTD, and reflected CTM, respectively, are given as

$$E_j=\frac{\left\langle P_j^*\right\rangle}{\left\langle P_0^*\right\rangle},\qquad (j=1,2,3), \tag{24}$$

where $\left\langle P_0^* \right\rangle$ denotes the average energy transmission per unit surface area per unit time for incident CLD wave in rotating nonlocal micropolar piezoelectric medium M.

The expressions for energy ratios at the interface $x_3 = 0$ are given as

$$E_j = \left(\frac{\hbar_{1j} + \hbar_{2j} - \hbar_{3j}}{\hbar_0} \right) Z_j^2, \qquad (j = 1,2,3) \tag{25}$$

where

$$\hbar_{1j} = \left(A_{13}\xi_j + A_{56}\xi_j - \lambda_{35}\xi_j\zeta_j - \lambda_{31}\zeta_j \right)\sin\theta_o,$$

$$\hbar_{2j} = -\left(A_{55} + A_{33}\xi_j^2 - \lambda_{33}\xi_j\zeta_j - \lambda_{35}\zeta_j + B_{66}\eta_j^2 \right)\sqrt{\left(\frac{v_1}{v_j} \right)^2 - \sin^2\theta_o},$$

$$\hbar_{3j} = i\left(A_{56} - A_{55} \right)\left(\frac{v_1}{v_j} \right)\left(\frac{\eta_j}{k_j} \right),$$

$$\hbar_0 = \begin{Bmatrix} \left(A_{13}\xi_1^* + A_{56}\xi_1^* - \lambda_{35}\xi_1^*\zeta_1^* - \lambda_{31}\zeta_1^* \right)\sin\theta_o + \\ (A_{55} + A_{33}\xi_1^{*2} - \lambda_{33}\xi_1^*\zeta_1^* - \lambda_{35}\zeta_1^* + B_{66}\eta_1^{*2})\cos\theta_o - i\left(A_{56} - A_{55} \right)\left(\frac{\eta_1^*}{k_1} \right) \end{Bmatrix}.$$

Particular cases

(a) In the absence of nonlocal parameter ($\varepsilon = 0$), the above theoretical analysis reduces for the case when a plane wave is incident at a traction-free boundary of a transversely isotropic rotating micropolar piezoelectric solid half-space.

(b) In the absence of rotation rate ($\Omega^* = 0$), the above theoretical analysis reduces for the case when a plane wave is incident at a traction-free boundary of a transversely isotropic nonlocal micropolar piezoelectric solid half-space.

(c) In absence of rotation and nonlocality ($\Omega^* = 0, \varepsilon = 0$), the above theoretical analysis reduces for the case when a plane wave is incident at a traction-free boundary of a micropolar piezoelectric solid half-space of transversely isotropic type.

Numerical results and discussion

For illustrations of speeds, amplitude ratios, and energy ratios, the following physical constants of a micropolar piezoelectric material are considered (Singh and Sindhu [59], Sangwan et al. [60])

$$A_{11} = 17.8\times10^{10}\,Nm^{-2},\ A_{33} = 18.43\times10^{10}\,Nm^{-2},\ A_{13} = 7.59\times10^{10}\,Nm^{-2},\ A_{56} = 1.89\times10^{10}\,Nm^{-2},$$

$$A_{55} = 4.357\times10^{10}\,Nm^{-2},\ A_{66} = 4.42\times10^{10}\,Nm^{-2},\ B_{77} = 2.78\times10^{10}\,N,\ B_{66} = 2.68\times10^{10}\,N,$$

$$\lambda_{15} = 1\times10^{-5}\,Cm^{-2},\ \lambda_{31} = 3.9\,Cm^{-2},\ \lambda_{33} = 1.33\,Cm^{-2},\ \lambda_{35} = 0.23\,Cm^{-2},\ \omega = 10^5\,Hz,$$

$$\gamma_{11} = 85.2\,C^2N^{-1}m^{-2},\ \gamma_{33} = 28.7\,C^2N^{-1}m^{-2},\ \rho = 1740\,Kg\,m^{-3},\ j = 0.196\,m^2.$$

For the above physical constants, Equations (15), (22), and (25) are solved numerically with the help of programming in MATLAB. The propagation speeds, the modulus of amplitude ratios, and energy ratios of various reflected waves are computed for different values of nonlocal parameter ε and rotation rate Ω^*. The CLD and CTM waves are observed as the fastest and slowest waves, respectively.

Speeds of plane waves

Speeds versus rotation parameter. To illustrate the effects of rotation and nonlocal parameters, the speeds of CLD, CTD, and CTM waves are plotted against rotation rate Ω^* ($0 \le \Omega^* < 1$) in Fig. 2 for three distinct nonlocal parameters when the angle of incidence θ_o is fixed as 45°. The solid, dashed, and dotted curves in Fig. 2 correspond to the speed variations of CLD, CTD, and CTM waves for the nonlocal parameter $\varepsilon = 0,\ 0.007,\ 0.008$, respectively. For $\varepsilon = 0,\ 0.007$ and 0.008, the speed of CLD wave as shown in Fig. 2(a) is approximately 0.96×10^4 ms^{-1} at $\Omega^* = 0$ and it increases uniformly as the rotation parameter Ω^* increases from 0 to 0.9. Beyond $\Omega^* = 0.9$, the speed of CLD wave increases very sharply to a maximum value 8.045×10^5 ms^{-1} at $\Omega^* = 0.99$. The speeds of CTD and CTM waves as illustrated in Fig. 2 decrease uniformly as Ω^* increases from 0 to 0.99. However, the rate of decrease in speed of CTM wave is very low as compared to CTD wave. From Figure 2, it is noticed that the speeds of CLD, CTD, and CTM waves become slow in the presence of nonlocal parameters.

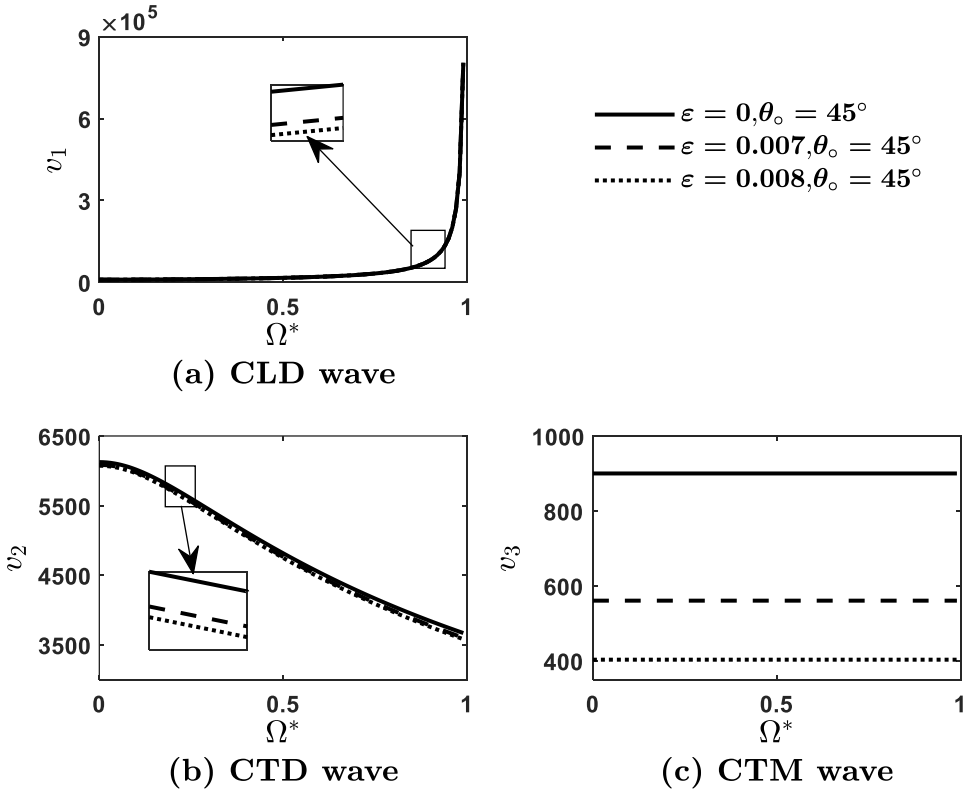

Fig. 2. The speed variations of CLD, CTD, and CTM waves against rotational rate for distinct nonlocal parameters

Speeds versus nonlocal parameters. To validate the rotation and nonlocality effects shown in Fig. 2 the speeds of CLD, CTD, and CTM waves are also plotted against nonlocal parameter ε shown in Fig. 3 for three different values of Ω^* when $\theta_o = 45^\circ$. The solid, dashed, and dotted curves in Fig. 3 correspond to variations in speeds of reflected CLD, CTD, and CTM waves for $\Omega^* = 0.1,\ 0.4,\ 0.8$, respectively. For each value of Ω^*, the speeds of CLD, CTD and CTM waves decrease as nonlocal parameter ε increases. Beyond the critical

values of nonlocal parameters, these waves do not exist. The range of nonlocal parameters for the propagation of these waves depends on the rotation parameter Ω^*. The range of nonlocal parameters for the existence of CLD increases as Ω^* increases, whereas the range of nonlocal parameters for the existence of CTD decreases as Ω^* increases. The CTM wave is little affected due to nonlocal as well as rotation parameters.

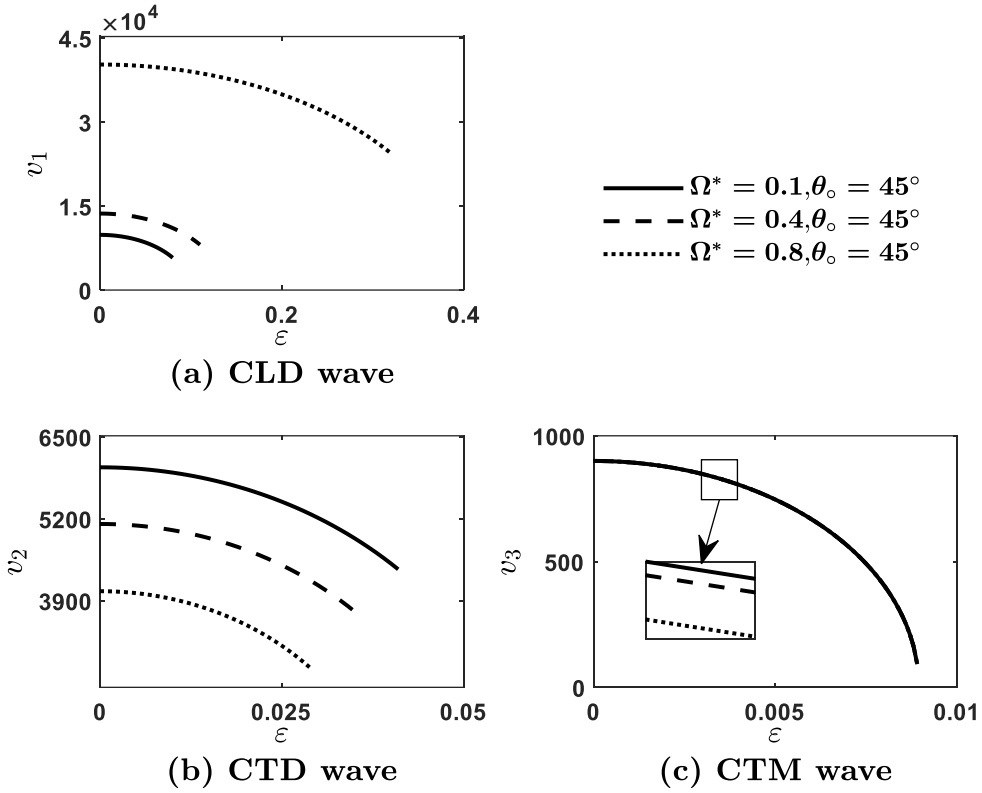

Fig. 3. The speed variations of CLD, CTD, and CTM waves against nonlocal parameters for distinct rotation rates

Speeds versus propagation angle. The speeds of CLD, CTD, and CTM waves are plotted against the propagation angle in Fig. 4 for three different nonlocal parameters when rotation rate $\Omega^* = 0.8$. The solid, dashed and dotted curves in these figures correspond to speed variations for $\varepsilon = 0$, 0.007 and 0.008, respectively. For $\varepsilon = 0$, the speed of CLD wave decreases from 4.0571×10^4 ms^{-1} at $\theta_o = 0.01^\circ$ (near normal incidence) to value 4.0060×10^4 ms^{-1} at $\theta_o = 89.99^\circ$ (near grazing incidence). For $\varepsilon = 0$, the speed of CTD wave first increases from 3533.74 ms^{-1} at $\theta_o = 0.01^\circ$ to its maximum value 4051.05 ms^{-1} at $\theta_o = 45.30^\circ$ and then decreases to value 3542.78 ms^{-1} at $\theta_o = 89.99^\circ$. For $\varepsilon = 0$, the speed of CTM wave increases slightly from 891.08 ms^{-1} at $\theta_o = 0.01^\circ$ to 907.48 ms^{-1} at $\theta_o = 89.99^\circ$. Similar speed variations of CLD, CTD, and CTM waves are also obtained for $\varepsilon = 0.007$ and 0.008 as shown in Fig. 4. The comparison of solid, dotted and dashed curves in these figures show the nonlocal effects on the speed of these waves at each propagation angle. A similar analysis of speed variations of CLD, CTD, and CTM waves is also shown in Fig. 5 to illustrate the effect of rotation in a given range of propagation angle when $\varepsilon = 0.001$.

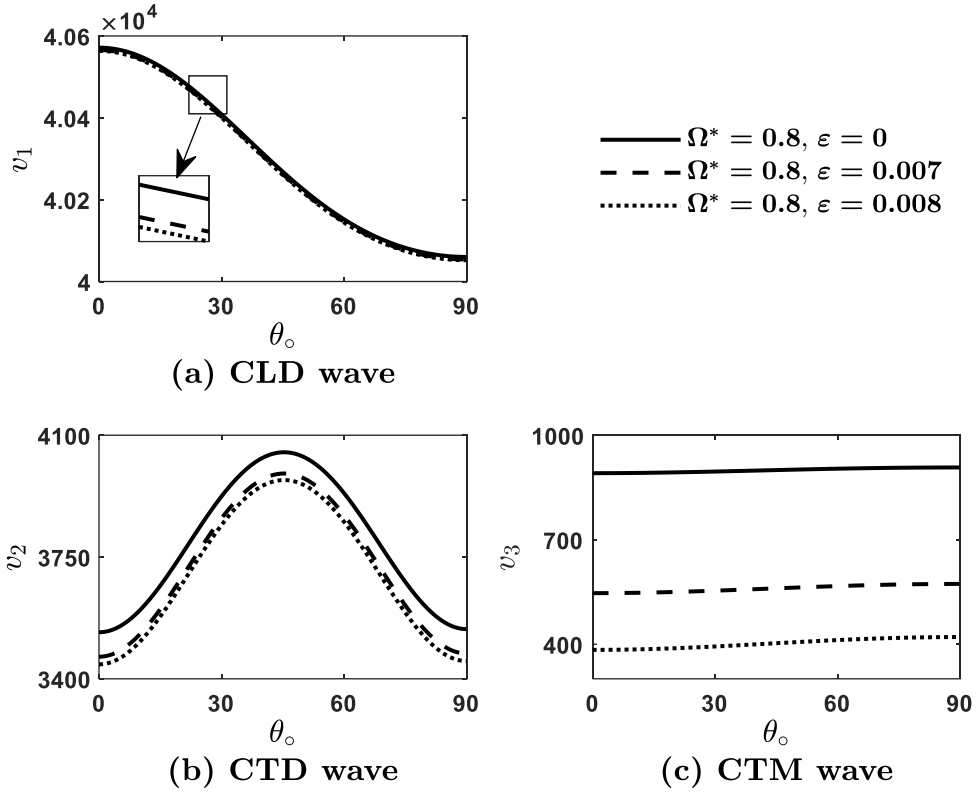

Fig. 4. The speed variations of CLD, CTD, and CTM waves against the incident angle of CLD wave for distinct nonlocal parameters when Ω^* = 0.8

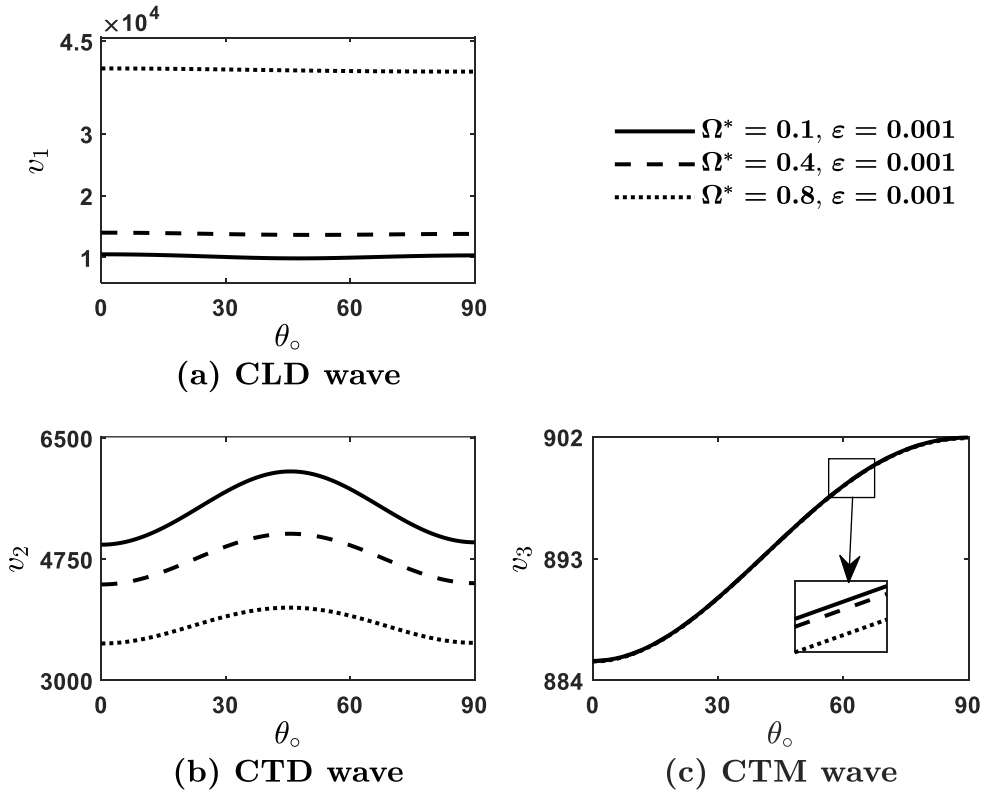

Fig. 5. The speed variations of CLD, CTD, and CTM waves against the incident angle of CLD wave for distinct rotation rates when ε = 0.001

Amplitude and energy ratios versus angle of incidence of CLD wave

The amplitude ratios $|Z_1|, |Z_2|$, and $|Z_3|$ of reflected CLD, CTD, and CTM waves are plotted against the incident angle θ_o of CLD wave in Fig. 6 for $\varepsilon = 0$ (solid curve), $\varepsilon = 0.007$ (dashed curve), and $\varepsilon = 0.008$ (dotted curve) when $\Omega^* = 0.8$.

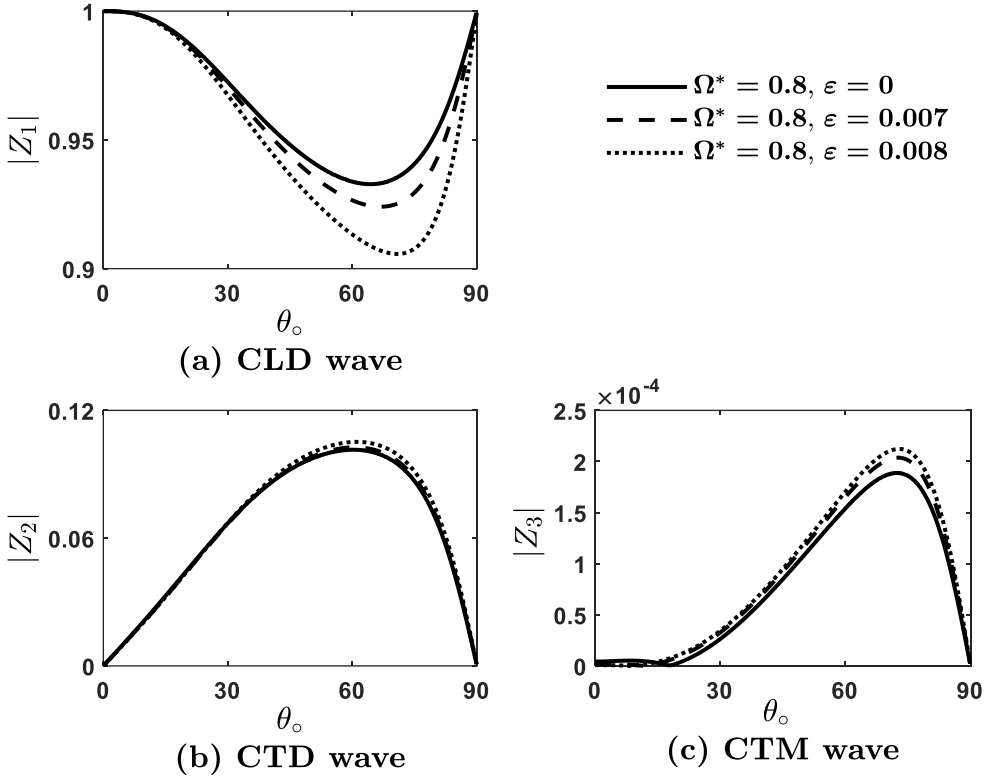

Fig. 6. The amplitude ratio variations of CLD, CTD, and CTM waves against the incident angle of CLD wave for distinct nonlocal parameters when $\Omega^* = 0.8$

For $\varepsilon = 0$, the amplitude ratio of reflected CLD wave decreases from 0.9999 at $\theta_o = 0.01^\circ$ to its minimum value 0.9328 at $\theta_o = 64.36^\circ$ and then increases to a value 0.9999 at $\theta_o = 89.99^\circ$. For $\varepsilon = 0$, the reflected CTD wave amplitude ratio increases from 2.1279×10^{-5} at $\theta_o = 0.01^\circ$ to its maximum value 0.1015 at $\theta_o = 60.23^\circ$ and then decreases to value 8.6324×10^{-5} at $\theta_o = 89.99^\circ$. For $\varepsilon = 0$, the amplitude ratio of the reflected CTM wave oscillates in the given range of incident angle. In the presence of nonlocality, the amplitude ratio of reflected CLD wave drops, and the amplitude ratios of CTD and CTM waves rise at each angle of incidence except the normal and grazing incidences. The maximum effect of nonlocality on these amplitude ratios is observed in the range between 60° to 80° of the incident angle. Similar amplitude ratio variations of reflected CLD, CTD, and CTM waves are also shown in Fig. 7 to illustrate the effect of rotation at each incident angle. The amplitude ratio of CLD wave rises and the amplitude ratios of CTD and CTM waves drop at each incident angle except the normal and grazing incidences.

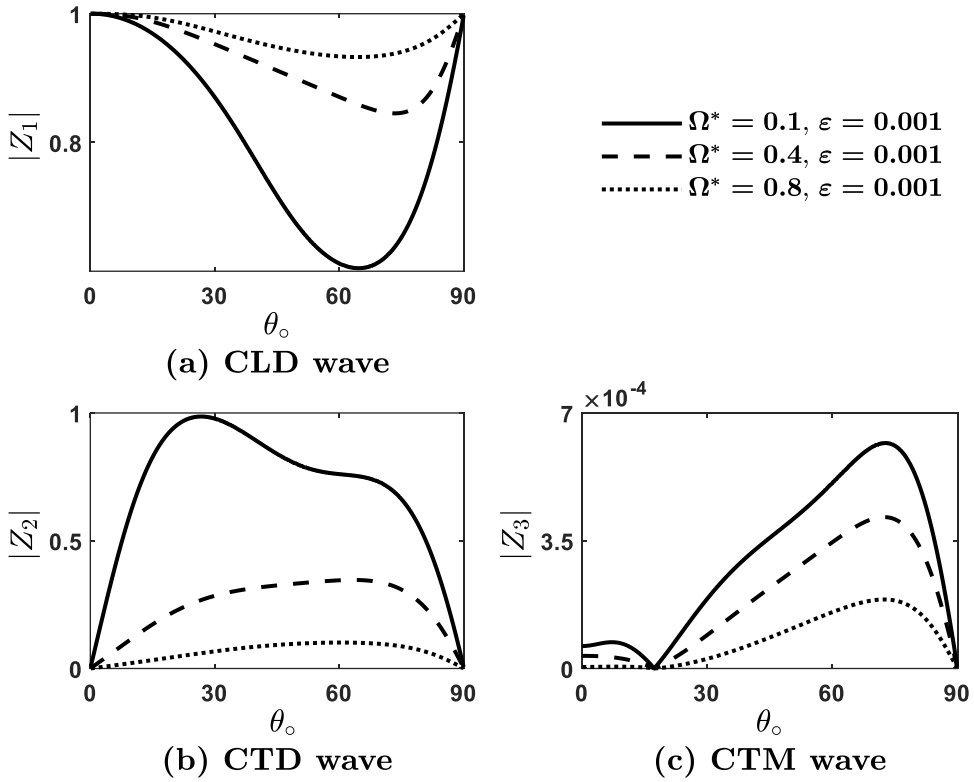

Fig. 7. The amplitude ratio variations of CLD, CTD, and CTM waves against the incident angle of CLD wave for distinct rotation rates when ε = 0.001

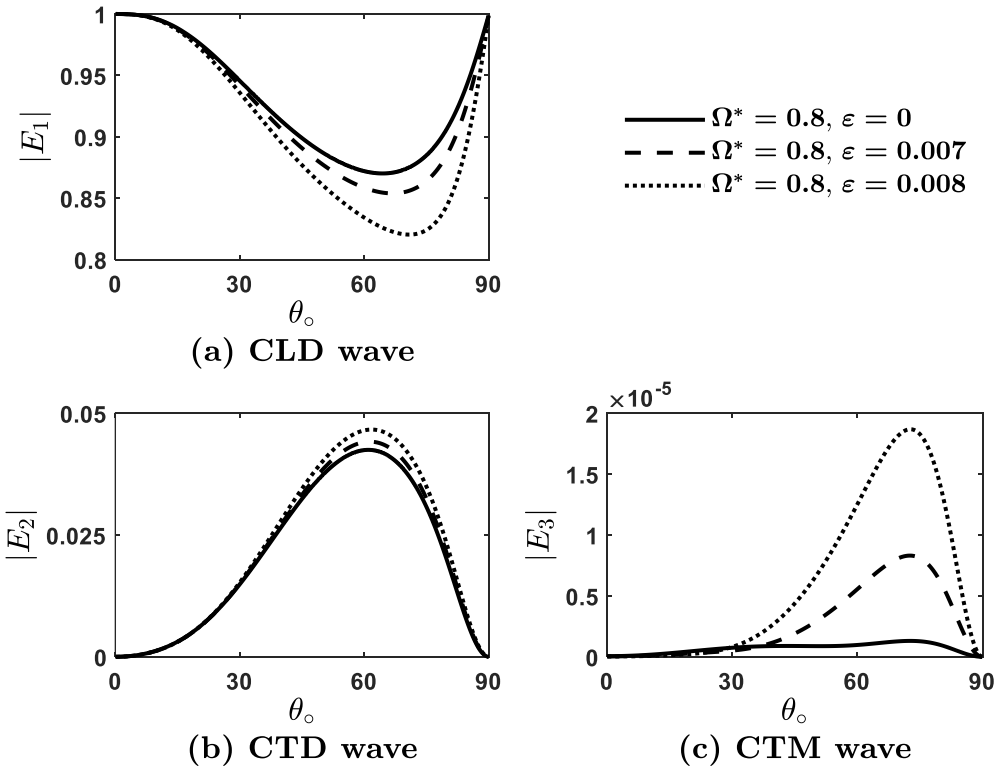

Fig. 8. The energy ratio variations of CLD, CTD, and CTM waves against the incident angle of CLD wave for distinct nonlocal parameters when Ω^* = 0.8

The energy ratio variations of the reflected CLD, CTD, and CTM are shown in Figs. 8 and 9 are observed similar to those of amplitude ratios. The nonlocality and rotation parameters affect the energy ratios of these reflected waves in a similar pattern as these parameters affect the amplitude ratios. The main aim of illustrating the energy ratio in Figs. 8 and 9 is to validate the numerical correctness of the amplitude ratio variations. From these figures, it is also noticed that the reflected CLD wave shares the maximum part of the energy ratio, and the reflected CTM wave shares the minimum and very little share of the energy ratio compared to other reflected waves. However, the energy shares of each reflected wave change with the incident angle.

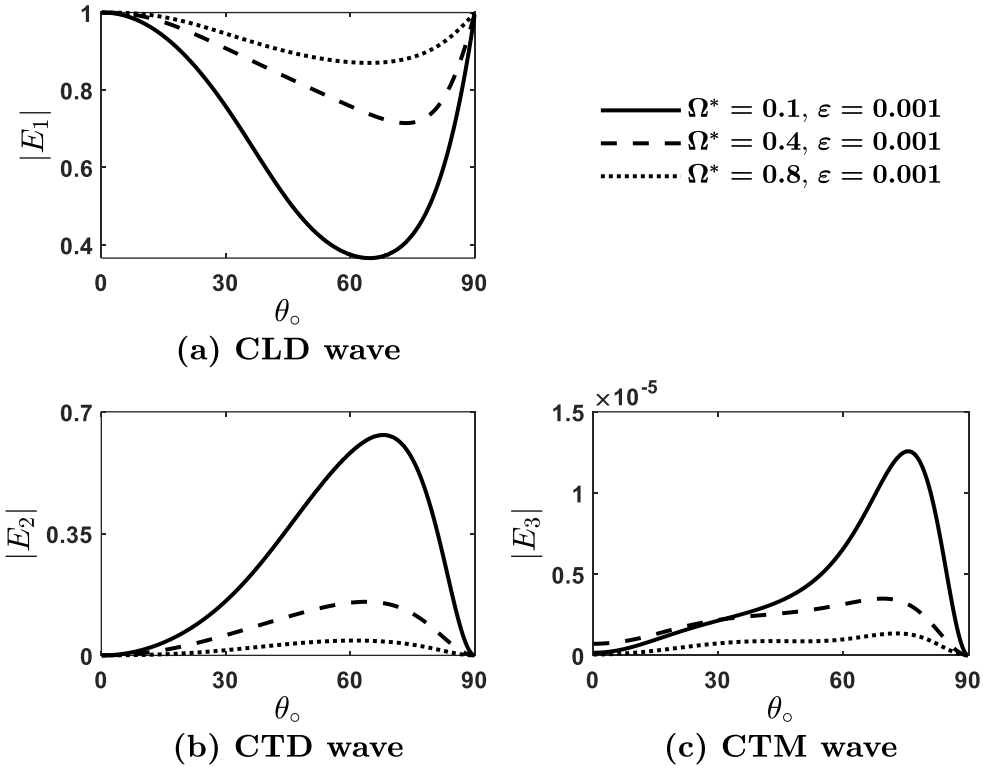

Fig. 9. The energy ratio variations of CLD, CTD, and CTM waves against the incident angle of CLD wave for distinct rotation rates when ε = 0.001

Conclusions

Plane waves in a rotating nonlocal micropolar piezoelectric medium are investigated. There exist three coupled waves, namely Coupled Longitudinal Displacement (CLD) wave, Coupled Transverse Displacement (CTD) wave and Coupled Transverse Microrotational (CTM) wave. The CLD and CTM waves are observed as the fastest and slowest waves, respectively. A reflection phenomenon of incident CLD wave from a tractions-free surface is considered. The relations between various reflected waves amplitude ratios are derived. The energy ratio expressions of these reflected waves are also derived. A numerical example is considered to illustrate the dependence of the speeds, amplitude, and energy ratios on the nonlocality and rotation parameters in a given range of the angle of incidence. Some specific observations from the numerical example are derived as follows:

1. For given rotation parameter Ω^* and propagation angles, the speeds of CLD, CTD, and CTM waves decrease as the nonlocal parameter ε increases.
2. For given nonlocal parameter ε and propagation angle, the speed of CLD wave increases, and the speeds of CTD and CTM waves decreases.

3. Beyond the critical values of the nonlocal parameter, the CLD, CTD, and CTM waves do not propagate. The range of nonlocal parameters for the propagation of these waves depends on the rotation parameter Ω^*. The range of nonlocal parameters for the existence of CLD increases as Ω^* increases, whereas the range of nonlocal parameters for the existence of CTD decreases as Ω^* increases. The CTM wave is little affected due to nonlocal as well as rotation parameters.
4. The speeds, amplitude ratios, and energy ratios vary with the change in propagation angle and the nonlocal and rotation effects are also found dependent on the propagation angle.

The present theoretical and numerical analysis may be used to estimate the possible nonlocal parameters for various nonlocal micropolar piezoelectric materials.

References

1. Knott CG. Reflexion and refraction of elastic waves with seismological applications. *Lond Edinb Dublin Philos Mag J Sci*. 1899;48: 64-97.
2. Jeffreys H. The reflexion and refraction of elastic waves. *Geophysical Suppl Mon Notices Royal Astron*. 1926;1(7): 321-334.
3. Gutenberg B. Energy ratio of reflected and refracted seismic waves. *Bull Seismol Soc Am.* 1944;34(2): 85-102.
4. Ergin K. Energy ratio of the seismic waves reflected and refracted at a rock-water boundary. *Bull Seismol Soc Am*. 1950;42(4): 349-372.
5. Ewing WM, Jardetzky WS, Press F. *Elastic waves in layered media*. New York: McGraw-Hill; 1957.
6. Achenbach JD. *Wave propagation in elastic solids*. New York: North-Holland; 1973.
7. Kyame JJ. Wave Propagation in piezoelectric crystals. *J Acoust Soc Am*. 1949;21(3): 159-167.
8. Pailloux PMH. Piézoélectricité Calcul des vitesses de propagation [Piezoelectricity. Calculation of propagation velocities]. *Le Journal De Physique Et Le Radium*. 1958;19:523-526. (In French)
9. Cheng NC, Sun CT. Wave propagation in two-layered piezoelectric plates. *J Acoust Soc Am*. 1975;57(3): 632-638.
10. Auld BA. Wave propagation and resonance in piezoelectric materials. *J Acoust Soc Am.* 1981;70(6): 1577-1585.
11. Alshits VI, Lothe J, Lyubimov VN. The phase shift for reflection of elastic waves in hexagonal piezoelectric crystals. *Wave Motion*. 1984;6(3): 259-264.
12. Parton VZ, Kudryavtsev BA. *Electromagnetoelasticity: piezoelectrics and electrically conductive solids*. New York: Gordon and Beach; 1988.
13. Every AG, Neiman VI. Reflection of electroacoustic waves in piezoelectric solids: Mode conversion into four bulk waves. *J Appl Phys*. 1992;71(12): 6018-6024.
14. Alshits VI, Shuvalov AL. Resonance reflection and transmission of shear elastic waves in multilayered piezoelectric structures. *J Appl Phys*. 1995;77(6): 2659-2665.
15. Wang Q. Wave propagation in a piezoelectric coupled solid medium. *J Appl Mech*. 2002;69: 819-824.
16. Yang JS. A review of a few topics in piezoelectricity. *Appl Mech Rev*. 2006;59: 335-345.
17. Pang Y, Wang YS, Liu JX, Fang DN. Reflection and refraction of plane waves at the interface between piezoelectric and piezomagnetic media. *Int J Eng Sci*. 2008;46(11): 1098-1110.
18. Darinskii AN, Clezio EL, Feuillard G. The role of electromagnetic waves in the reflection of acoustic waves in piezoelectric crystals. *Wave Motion*. 2008;45(4): 428–444.

19. Burkov SI, Sorokin BP. Aleksandrov KS, Karpovich AA. Reflection and refraction of bulk acoustic waves in piezoelectrics under uniaxial stress. *Acoust Phys*. 2009;55: 178–185.
20. Abd-alla AN, Al-sheikh FA. Reflection and refraction of plane quasi-longitudinal waves at an interface of two piezoelectric media under initial stress. *Arch Appl. Mech*. 2009;79: 843-857.
21. Singh B. Wave propagation in a prestressed piezoelectric half-space. *Acta Mech.* 2010;211: 337-344.
22. Kuang ZB, Yuan XG. Reflection and transmission of waves in pyroelectric and piezoelectric materials. *J Sound Vib*. 2011;330(6): 1111-1120.
23. Yuan X, Zhu ZH. Reflection and refraction of plane waves at interface between two piezoelectric media. *Acta Mech*. 2012;223: 2509-2521.
24. Guo X, Wei P. Effects of initial stress on the reflection and transmission waves at the interface between two piezoelectric half spaces. *Int J Solids Struct*. 2014;51(21-22): 3735-3751.
25. Guo X, Wei P, Li L, Tang Q. Influences of mechanically and dielectrically imperfect interfaces on the reflection and transmission waves between two piezoelectric half spaces. *Int J Solids Struct.* 2015;63: 184-205.
26. Othman MIA, Elmaklizi YD, Ahmed EAA. Influence of magnetic field on generalized piezo-thermoelastic rotating medium with two relaxation times. *Microsyst Technol*. 2017;23: 5599–5612.
27. Singh B, Singh B. Reflection from free surface of a rotating generalized thermo-piezoelectric solid half space. *J Solid Mech*. 2018;10(1): 57-66.
28. Jiao F, Wei P, Zhou Y, Zhou X. Wave propagation through a piezoelectric semiconductor slab sandwiched by two piezoelectric half-spaces. *Eur J Mech A Solids*. 2019;75: 70-81.
29. Sahu SA, Nirwal S, Mondal S. Reflection and transmission of quasi-plane waves at the interface of piezoelectric semiconductors with initial stresses. *Appl Math Mech.* 2021;42(7): 951–968.
30. Singh S, Singh AK, Guha S. Impact of interfacial imperfections on the reflection and transmission phenomenon of plane waves in a porous-piezoelectric model. *Appl Math Model.* 2021;100: 656-675.
31. Liu C, Yu J, Wang X, Zhang B, Zhang X, Zhou H. Reflection and transmission of elastic waves through nonlocal piezoelectric plates sandwiched in two solid half-spaces. *Thin-Walled Struct*. 2021;168: 108306.
32. Schoenberg M, Censor D. Elastic waves in rotating media. *Q Appl Math*. 1973;31: 115-125.
33. White RW. Acoustic sensors for physical, chemical and biochemical applications. In: *Proceedings of the 1998 IEEE International Frequency Control Symposium*. 1998. p.587–594.
34. Tiersten HF, Stevens DS, Das PK. Acoustic surface wave accelerometer and rotation rate sensor. In: *1980 Ultrasonics Symposium.* Bosten (MA): IEEE; 2005. p.692–695.
35. Tiersten HF, Stevens DS, Das PK. Circulating flexural wave rotation rate sensor. In: *1981 Ultrasonics Symposium*. Chicago (IL): IEEE; 2005. p.163–166.
36. Wren T, Burdess JS. Surface waves perturbed by rotation. *ASME J. Appl Mech.* 1987;54: 464–466.
37. Edelen DGB, Green AE, Laws N. Nonlocal continuum mechanics. *Arch Ration Mech Anal.* 1971;43: 36-44.
38. Eringen AC, Edelen DGB. On nonlocal elasticity. *Int J Eng Sci*. 1972;10: 233-248.
39. Eringen AC. *Nonlocal continuum field theories*. New York: Springer; 2001.
40. Eringen AC. Linear theory of nonlocal elasticity and dispersion of plane waves. *Int J Eng Sci*. 1972;10(5): 425–435.

41. Eringen AC. Plane waves in nonlocal micropolar elasticity. *Int J Eng Sci*. 1984;22: 1113-1121.
42. Roy I, Acharya DP, Acharya S. Rayleigh wave in a rotating nonlocal magnetoelastic half-plane. *J Theor Appl Mech*. 2015;45: 61-78.
43. Khurana A, Tomar SK. Reflection of plane longitudinal waves from the stress-free boundary of a nonlocal, micropolar solid half-space. *J Mech Mater Struct*. 2013;8: 95-107.
44. Khurana A, Tomar SK. Wave propagation in nonlocal microstretch solid. *Appl Math Model*. 2016;40: 5858-5875.
45. Singh B. Rayleigh-type surface waves in a nonlocal thermoelastic solid half space with voids. *Waves Random Complex Media*. 2021;31(6): 2103-2114.
46. Singh B. Propagation of waves in an incompressible rotating transversely isotropic nonlocal elastic solid. *Vietnam J Mech.* 2021;43(3): 237-252.
47. Kaur B, Singh B. Rayleigh-type surface wave in nonlocal isotropic diffusive materials. *Acta Mech.* 2021;232: 3407-3416.
48. Tung DX. The reflection and transmission of a quasi-longitudinal displacement wave at an imperfect interface between two nonlocal orthotropic micropolar half-space. *Arch Appl Mech*. 2021;91: 4313-4328.
49. Eringen AC. Linear theory of micropolar elasticity. *J Math Mech*. 1966;15: 909-923.
50. Eringen AC. *Theory of micropolar elasticity. Fracture 2.* New York: Academic Press; 1968.
51. Eringen AC. *Microcontinuum field theories I: foundations and solids*. New York: Springer; 1999.
52. Cracium IA. Uniqueness theorem in the linear theory of piezoelectric micropolar thermoelasticity ion. *Int J Eng Sci*. 1995;33: 1027-1036.
53. Ciumasu SG, Vieru D. Variational formulations for the vibration of a micropolar piezoelectric body. *J Acoust Soc Am*. 1999;105: 1240.
54. Vieru D, Ciumasu SG. Love waves in non-classical micropolar piezoelectricity. *J Acoust Soc Am*. 1999;105: 1241.
55. Zhilin PA, Kolpakov YE. A micro-polar theory for piezoelectric materials. In: *Lecture at XXXIII Summer School–Conference-Advanced Problems in Mechanics*. St. Petersburg, Russia; 2015.
56. Aouadi M. Aspects of uniqueness in micropolar piezoelectric bodies. *Math Mech Solids.* 2008;13: 499-512.
57. Gales C. Some results in micromorphic piezoelectricity. *Eur J Mech A Solids.* 2012;31: 37-46.
58. Singh B, Sindhu R. On propagation of Rayleigh type surface wave in a micropolar piezoelectric medium. *Open J Acoust*. 2016;6(4): 35-44.
59. Singh B, Sindhu R. Rotational effects on propagation of Rayleigh wave in a micropolar piezoelectric medium. *J Theor Appl Mech*. 2018;48: 93-105.
60. Sangwan A, Singh B, Singh J. Reflection and transmission of plane waves at an interface between elastic and micropolar piezoelectric solid half-spaces. *Tech Mech*. 2018;38(3): 267-285.
61. Singh B, Sangwan A, Singh J. Reflection and transmission of elastic waves at an interface between two micropolar piezoelectric half-spaces. *J Ocean Eng Sci.* 2019;4(3): 227-237.
62. Bijarnia R, Singh B, Awrejcewicz J. Reflection at non-free boundary of a micropolar piezoelectric half-space. *Forces Mech.* 2021;3: 100019

THE AUTHORS

Baljeet Singh
e-mail: bsinghgc11@gmail.com

Asha Sangwan
e-mail: aashisangwan53@gmail.com

Jagdish Singh
e-mail: jsnandal2k15@gmail.com

Appendix

The expressions for $\xi_1^*, \eta_1^*, \zeta_1^*, \xi_p, \eta_p$ and $\zeta_p\,(p=1,2,3)$ using Snell's law are given as

$$\xi_1^*=\frac{\Delta_1^*}{\Delta},\ \frac{\eta_1^*}{k_1}=\frac{\Delta_2^*}{\Delta},\ \zeta_1^*=\frac{\Delta_3^*}{\Delta},\ \xi_p=\frac{\Delta_{1p}}{\Delta_p},\ \frac{\eta_p}{k_p}=\frac{\Delta_{2p}}{\Delta_p},\ \zeta_p=\frac{\Delta_{3p}}{\Delta_p},$$

where

$$\Delta_p=\begin{vmatrix} C_p & K_{1p} & G_p \\ Q_p & K_{2p} & T_p \\ K_{2p}^* & R_p & 0 \end{vmatrix},\ \Delta_{1p}=\begin{vmatrix} P_p & K_{1p} & G_p \\ F_p & K_{2p} & T_p \\ K_{1p}^* & R_p & 0 \end{vmatrix},$$

$$\Delta_{2p}=\begin{vmatrix} C_p & P_p & G_p \\ Q_p & F_p & T_p \\ K_{2p}^* & K_{1p}^* & 0 \end{vmatrix},\ \Delta_{3p}=\begin{vmatrix} C_p & K_{1p} & P_p \\ Q_p & K_{2p} & F_p \\ K_{2p}^* & R_p & K_{1p}^* \end{vmatrix},$$

$$\Delta=\begin{vmatrix} C_0 & -K_{11} & -G_1 \\ Q_1 & K_{21} & T_1 \\ K_{21}^* & R_1 & 0 \end{vmatrix},\ \Delta_1^*=\begin{vmatrix} P_1 & -K_{11} & -G_1 \\ F_0 & K_{21} & T_1 \\ -K_{11}^* & R_1 & 0 \end{vmatrix},$$

$$\Delta_2^*=\begin{vmatrix} C_0 & P_1 & -G_1 \\ Q_1 & F_0 & T_1 \\ K_{21}^* & -K_{11}^* & 0 \end{vmatrix},\ \Delta_3^*=\begin{vmatrix} C_0 & -K_{11} & P_1 \\ Q_1 & K_{21} & F_0 \\ K_{21}^* & R_1 & -K_{11}^* \end{vmatrix},$$

where

$$P_p=\left[1+\left(\Omega^*\right)^2\right]\left(\rho v_p^2+\rho\varepsilon^2\omega^2\right)-A_{11}\sin^2\theta_o\left(\frac{v_p}{v_1}\right)^2-A_{55}\left[1-\sin^2\theta_o\left(\frac{v_p}{v_1}\right)^2\right],$$

$$Q_p=\left[1+\left(\Omega^*\right)^2\right]\left(\rho v_p^2+\rho\varepsilon^2\omega^2\right)-A_{66}\sin^2\theta_o\left(\frac{v_p}{v_1}\right)^2-A_{33}\left[1-\sin^2\theta_o\left(\frac{v_p}{v_1}\right)^2\right],$$

$$R_p=\frac{B_{77}}{j}\sin^2\theta_o\left(\frac{v_p}{v_1}\right)^2+\frac{B_{66}}{j}\left[1-\sin^2\theta_o\left(\frac{v_p}{v_1}\right)^2\right]+\frac{\chi}{jk_p^2}-\left(\rho v_p^2+\rho\varepsilon^2\omega^2\right),$$

$$T_p=\lambda_{15}\sin^2\theta_o\left(\frac{v_p}{v_1}\right)^2+\lambda_{33}\left[1-\sin^2\theta_o\left(\frac{v_p}{v_1}\right)^2\right],$$

$$C_p=-\left(A_{13}+A_{56}\right)\sin\theta_o\left(\frac{v_p}{v_1}\right)\sqrt{1-\sin^2\theta_o\left(\frac{v_p}{v_1}\right)^2}-2i\,\Omega^*\left(\rho v_p^2+\rho\varepsilon^2\omega^2\right),$$

$$C_0=\left(A_{13}+A_{56}\right)\sin\theta_o\cos\theta_o-2i\,\Omega^*\left(\rho v_1^2+\rho\varepsilon^2\omega^2\right),$$

$$F_p=-\left(A_{13}+A_{56}\right)\sin\theta_o\left(\frac{v_p}{v_1}\right)\sqrt{1-\sin^2\theta_o\left(\frac{v_p}{v_1}\right)^2}+2i\,\Omega^*\left(\rho v_p^2+\rho\varepsilon^2\omega^2\right),$$

$$F_0=\left(A_{13}+A_{56}\right)\sin\theta_o\cos\theta_o+2i\,\Omega^*\left(\rho v_1^2+\rho\varepsilon^2\omega^2\right),$$

$$G_p=\left(\lambda_{15}+\lambda_{31}\right)\sin\theta_o\left(\frac{v_p}{v_1}\right)\sqrt{1-\sin^2\theta_o\left(\frac{v_p}{v_1}\right)^2},\quad \Omega^*=\frac{\Omega}{\omega},$$

$$K_{1p} = iK_1\sqrt{1-\sin^2\theta_o\left(\frac{v_p}{v_1}\right)^2},\ K_{2p} = iK_2\sin\theta_o\left(\frac{v_p}{v_1}\right),$$

$$K^*_{1p} = i\frac{K_1}{jk_p^2}\sqrt{1-\sin^2\theta_o\left(\frac{v_p}{v_1}\right)^2},\ K^*_{2p} = i\frac{K_2}{jk_p^2}\sin\theta_o\left(\frac{v_p}{v_1}\right).$$